Available online at www.sciencedirect.com
ScienceDirect
Ceramics International 34 (2008) 573–580
CERAMICS INTERNATIONAL
www.elsevier.com/locate/ceramint

Influence of chrome-bearing sols vacuum impregnation on the properties of magnesia-chrome refractory

Yong-Yue Deng *, Hou-Zhi Wang, Hui-Zhong Zhao

The Hubei Province Key Laboratory of Refractories and Ceramics Ministry-Province Jointly Constructed Cultivation Base for State Key Laboratory, Wuhan University of Science and Technology, Wuhan 430081, Hubei Province, PR China

Received 25 November 2005; received in revised form 2 November 2006; accepted 18 December 2006
Available online 30 January 2007

Abstract

Two kinds of nanosized chrome-bearing sols, i.e. Cr_2O_3 precursor sol and $MgCr_2O_4$ spinel precursor sol, were obtained by homogeneous precipitation. Properties of the sol vacuum impregnated magnesia-chrome refractory, such as bulk density, cold crushing strength, pore distribution, and chemical composition, etc., are superior to those of the un-impregnated sample. SEM micrographs show a different microstructure of the impregnated sample as compared to the un-impregnated one. The influence of vacuum impregnation on copper slag corrosion resistance of magnesia-chrome refractories has also been evaluated. The results show that both sols could improve the magnesia-chrome bricks corrosion resistance in impregnation.

Keywords: Chrome-bearing sol; Vacuum impregnation; Corrosion resistance; Magnesia-chrome refractory

1. Introduction

Owing to their high temperature stability, low thermal expansivity, and outstanding erosion-resisting performance [1], magnesia-chrome refractories have made their way in industries of iron and steel, cement, and copper smelting. In fact, magnesia-chrome brick is a major refractory material frequently used in the copper smelting industry [2–4]. Main wear mechanisms applied in the refractories of copper smelting furnaces include chemical attack, mechanical shock and damage caused by thermal spalling [3]. Since the refractories are susceptible to penetration by molten slag [4], damages on the refractories' internal structure (e.g. on copper converter) often ensue. Provided that thermodynamic factors are not to be considered, erosion the refractories suffer is determined by the contact surface [5]. And open pores are the leading contributor to the increased contacted surface. As the molten slag penetrates the pores of refractories, the ensuing migration will expand the contact surface of the refractories and the molten slag, rendering the refractories vulnerable to corrosion by the molten slag.

If the pressure factor is not taken into account, the velocity of molten slag penetrating through the pores can be obtained by the following equation [6]:

$$X = A\sqrt{\frac{r\sigma\cos\theta}{\eta}\tau} \quad (1)$$

where X is the infiltration depth; A the constant; r the pore radius; σ the Molten slag's surface tension; η the Molten slag's viscosity; τ the time; θ is the wetting angle.

According to equation above, the infiltration depth is in direct proportion to pore radius by decreasing the pore number and minifying the pore diameter, we will be capable of improving the material resistance against molten slag corrosion.

As we know pores exist in the materials in several types, including enclosed, blind and through, etc. [7]. All of them can have influence upon the material properties. Pores in the magnesia-chrome bricks usually have diameters ranging from 1 to 20 μm. Since the particles in sol are nanosized, they would have little difficulty getting into the material through pores or capillaries with the presence of pressure difference between the inside and the outside. As a rule, nanosized particles are linked with water molecules. After a refractory has been

* Corresponding author. Tel.: +86 27 68862160.
E-mail address: yongyuedeng@163.com (Y.-Y. Deng).

0272-8842/$34.00
doi:10.1016/j.ceramint.2006.12.002

treated with vacuum impregnation and dried at 100 °C (or higher), water molecules are vaporized. The nanosized particles may grow in size due to high temperature or develop into large aggregates that will remain in the pores, thereby decreasing the pores diameters. In summary, impregnating refractories with nanosized sol in vacuum state features the following merits:

1. Reduces the pore number and improving the pore structure of materials;
2. Decrease the pore diameter and occludes the through pores;
3. Lowers the apparent porosity.

Thus, we will be in a position to decrease the velocity and depth of the molten slag infiltration into the refractories as long as the sol impregnation can work to minify the pore diameter.

For the sake of this paper, the homogeneous precipitation method has been employed in fabricating the Cr_2O_3 precursor sol as well as the $MgCr_2O_4$ spinel precursor sol. By subjecting magnesia-chrome refractories to vacuum impregnation, we have studied and compared the slag resistance of the magnesia-chrome refractories before and after impregnation.

2. Experimental procedures

2.1. Test preparation

Burnt magnesia-chrome bricks from Luoyang Refractory Materials Factory (Henan, China) were used for test. In pursuance of relevant standards, the performance test was conducted on these bricks, with the major performance indicators set out in Table 1. In order to evaluate the physical and chemical properties after the vacuum impregnation, some of the bricks were cut into 40 mm × 40 mm × 40 mm test samples. In slag resistance evaluation, we resorted to the static crucible process [8]. Next, for the purpose of comparing slag resistance before and after the vacuum impregnation, another bricks were cut into 70 mm × 70 mm × 70 mm cubicles and bored on them round holes, 36 mm in width and 40 mm in depth. These samples were exposed to a copper smelting converter slag. Refer to Table 2 for the chemical compositions of the converter slag.

The chromium hydrate (single sol) and the magnesium and chromium hydrate (mixed sol) were both prepared following the homogeneous precipitation method, with urea as the precipitating agent [9]. Detailed below is the sol fabrication method taken:

Table 1
Properties of magnesite-chrome refractory brick

Chemical properties		Physical properties	
Constituents	Contents (wt%)		
MgO	74.81	Cold crushing strength (MPa)	68
Fe_2O_3	5.62	Bulk density (g cm^{-3})	3.192
Cr_2O_3	16.25	Apparent porosity (%)	15.8
SiO_2	1.37		
CaO	1.18		

Table 2
Chemical compositions of copper converter slag

Composition	%
Cu	1.64
Fe	56.55
S	0.26
Si	16.49
Zn	1.80
As	0.01
Pb	0.64

- Single sol: Based on the ratio $Mol_{(CCH)}$:$Mol_{(urea)}$ = 1:4, chromium chloride hexahydrate (shortened to CCH, purity 98%) and urea (purity 98%) were used to prepare a solution with the 2.0 mol/L concentration. After that, the solution was stirred on the mixing platform until all deposits dissolved. Next, the stirred solution was heated in a water bath box using temperatures 80–90 °C. When the pH of the solution reached 3.0, we took out the solution for use. As can be seen from the chemical equations (2) and (3), some $Cr(OH)_3$ particles exist in the solution.

$$CO(NH_2)_2 + 2H_2O \rightarrow CO_2 + 2NH_3{\cdot}H_2O \rightarrow 2NH_4^+ + 2OH^- \quad (2)$$

$$Cr^{3+} + 3OH^- \rightarrow Cr(OH)_3 \quad (3)$$

- Mixed sol: Based on the ratio $Mol_{(CCH)}$:$Mol_{(MCH)}$:$Mol_{(urea)}$ = 1:2:6, chromium chloride hexahydrate, magnesium chloride hexahydrate (shortened to MCH, purity 98%), urea (purity 98%) were used to prepare a solution with the 2.0 mol/L concentration. After that, the solution was stirred on the mixing platform until all deposits dissolved. Next, the stirred solution was heated in a water bath box using temperatures 80–90 °C. When the pH of the solution reached 3.5, we took out the solution for use.

2.2. Vacuum impregnation

First, the samples were placed in a pressure vessel, which was later evacuated until the pressure reached −0.1 MPa; the pressure had been maintained for 5–10 min. Next, under the room temperature, making use of the pressure difference between the inside and the outside, we refilled the single or mixed sol till the samples were immerged. With the pressure of −0.1 MPa, we waited for another 5 min [10]. Then, the samples were taken out and immediately placed in a drying stove. They were kept there for 24 h at 110 °C.

2.3. Test method and properties characterization

Some of the test samples were preserved for 3 h in the high-temperature furnace under 1000 and 1550 °C. At least three samples (40 mm × 40 mm × 40 mm) were averaged for

calculating the chemical and physical properties of the impregnated samples. Two impregnated and un-impregnated samples, after dried at 110 °C, were put to the slag resistance test. With an eye to ensure reliable comparison of the slag resistant property, 60 g copper converter slag (ground into 0.01 mm beforehand) was added to each sample, which was then heat-treated at 1600 °C in air for 3 h.

By the aid of a mercury porosimeter (AutoPore IV 9500 (Micromeritics), America), which allows measurement of porosity with pore diameters ranging from 0.005 to 360 μm, we measured the porosity and pore diameter distribution before and after impregnation. The bulk density and the apparent porosity of the samples treated at different temperatures were tested by means of the Archimedes Method (using kerosene as the fluid medium); the cold crushing strength was measured at room temperature by standard testing methods. The corrosion resistance was evaluated by comparing the depth and width of the slag attack on samples cut into halves, before and after impregnation; then slag resistance changes occurred in the samples microstructure and the profile of slag attack were evaluated by SEM (Philips XL-30TMP) at an accelerating voltage of 25.0 kV.

3. Results and discussion

3.1. Physical and chemical properties

The physical and chemical properties of the impregnated samples are set out in Table 3. Obviously, the content of Cr_2O_3 and the bulk density of the sol impregnated samples both have increased while the apparent porosity decreases. We will focus our attention on the single sol impregnation and explain the changes of properties. Since particles contained in the sol are nanosized (or smaller), they would have little difficulty entering the samples pores or capillaries when there is pressure difference. The incoming particles will then adhere to the uneven internal wall of the pores. While $Cr(OH)_3$ and Cr^{3+} particles exist in abundance in the single sol, $Cr(OH)_3$, crystal water aggregates, and Cr^{3+} particles constitute the majority of particles penetrating with the presence of vacuum. Having been dried at 110 °C, the samples continue to react with OH^- (resulting from the decomposition of urea), and generate more $Cr(OH)_3$, which start decomposition at 300 °C. As a result, the apparent porosity decreases significantly after the drying process at 110 °C. When the treatment temperature rises to 1000 °C, $Cr(OH)_3$ first loses the crystal water, then decomposes into nanosized Cr_2O_3, and finally gets crystallized to grow in size. Meanwhile, most Cl^- is vaporized. As we know, the molecule diameter of chromic hydroxide is larger than that of Cr_2O_3, thus, the original $Cr(OH)_3$ filling the pore gaps is replaced by Cr_2O_3 of smaller size. Despite the growing Cr_2O_3 crystal grains, the growth cannot offset the pore diameter changes, which are jointly contributed to by the minifying volume, the Cl^- evaporation, and the decomposition of remaining urea. And this accounts for why the pore diameters of the samples treated at 1000 °C are greater than those of the samples treated at 110 °C. With the treatment temperature reaching 1550 °C (much higher than temperature of the copper smelting furnace), some Cr particles are vaporized. Consequently, the Cr_2O_3 content and the bulk density both decline while the apparent porosity rises. On the other hand, according to Table 3, even with the heat-treatment at 1550 °C, the mixed sol impregnated samples feature a Cr_2O_3 content and a bulk density both higher than those of the samples impregnated in the single sol, and present a relatively lower apparent porosity. And this should be ascribed to a certain amount of Mg^{2+} in the mixed sol. Although the reaction described by Eq. (4) is not likely to occur due to low pH value during the heating in the water bath box, Mg^{2+} in the sol joins $Cr(OH)_3$ because of the action of Cl^-, making it undisputed that there do exist some Mg^{2+} in the sample impregnated. After the samples get dried at 110 °C, Mg^{2+} and OH^-, which results from the decomposition of the urea remaining in the samples' pores, engage into the reaction described by Eq. (4), producing $Mg(OH)_2$. Hence, after the heat-treatment at 110 °C, pores of the mixed sol impregnated samples are filled by a mixture of $Mg(OH)_2$ and $Cr(OH)_3$.

$$Mg^{2+} + 2OH^- \rightarrow Mg(OH)_2 \quad (4)$$

At temperature higher than 300 °C, $Cr(OH)_3$ and $Mg(OH)_2$ decompose to nanosized Cr_2O_3 and MgO, which, under the oxidative atmosphere, react at a lower temperature (600 °C), forming nanosized $MgCr_2O_4$, which grows at increasing temperature [11]. Due to low Cr vapor pressure in $MgCr_2O_4$, even with 1550 °C, the Cr evaporation rate in $MgCr_2O_4$ is lower than Cr in Cr_2O_3. In addition, compared with Cr_2O_3, $MgCr_2O_4$ particles occupy a larger volume. For this reason, the mixed sol impregnated samples show a higher bulk density but a lower apparent porosity than those impregnated in single sol.

Table 3
Chemical and physical properties of impregnated samples

Type		wt (%)		Cold crushing strength (MPa)	Bulk density (g cm^{-3})	Apparent porosity (%)
		MgO	Cr_2O_3			
Single sol	110 °C, 24 h	72.06	18.11	62	3.226	11.6
	1000 °C, 3 h	–	–	54	3.212	13.4
	1550 °C, 3 h	73.15	17.06	73	3.205	14.6
Mixed sol	110 °C, 24 h	75.92	17.03	65	3.231	9.8
	1000 °C, 3 h	–	–	41	3.218	12.6
	1550 °C, 3 h	75.48	16.77	67	3.214	13.9

Table 4
Porosimetric analysis before and after impregnation

Investigated types			Prior to impregnation	Single sol	Mixed sol
Total pore area ($m^2\ g^{-1}$)		110 °C, 24 h	0.0470	0.0379	0.0309
		1000 °C, 3 h	0.0500	0.0396	0.0390
		1550 °C, 3 h	0.0457	0.0400	0.0400
Median pore diameter (volume) (μm)		110 °C, 24 h	21.56	6.52	3.75
		1000 °C, 3 h	20.96	11.63	8.24
		1550 °C, 3 h	22.03	14.75	13.31
Median pore diameter (area) (μm)		110 °C, 24 h	0.77	0.42	0.24
		1000 °C, 3 h	0.74	0.36	0.27
		1550 °C, 3 h	0.80	0.66	0.67
Porosity (%)		110 °C, 24 h	14.60	9.39	7.93
		1000 °C, 3 h	13.89	15.31	10.35
		1550 °C, 3 h	15.07	14.97	13.61
Permeability (mdarcy)		110 °C, 24 h	64.32	9.84	14.63
		1000 °C, 3 h	56.59	47.46	12.92
		1550 °C, 3 h	55.31	47.89	36.10
Tortuosity (–)		110 °C, 24 h	9.23	47.50	69.44
		1000 °C, 3 h	12.85	25.18	36.11
		1550 °C, 3 h	10.32	23.36	17.81
Amount of pores (volume) (%)	110 °C, 24 h	>12 μm	89.52	21.69	18.64
		<12 μm	10.48	78.31	81.36
	1000 °C, 3 h	>12 μm	90.35	24.95	33.10
		<12 μm	9.65	75.05	66.90
	1550 °C, 3 h	>12 μm	90.74	75.80	72.45
		<12 μm	9.26	24.20	27.55

According to some Ref. [12], properties of the magnesia-chrome brick are subject to deterioration when treated with water-soluble solutions (e.g. cold crushing strength decreased noticeably). With a view to verify this, the cold crushing strength of the two sol-impregnated samples was tested. By comparing data set out in Tables 1 and 3, however, we only found minor strength discrepancy between the sol-impregnated sample and that not impregnated. This may result from the fact that the impregnation during the test process was well-timed and as a result, the possible adverse influence was avoided. Hence, concrete applications in future production are promised.

3.2. Pore diameter distribution before and after impregnation

Change of the distortion rate index is correlated to change of the pore structures in some way [13], as a higher distortion rate indicates a more complex pore structure. Accordingly, a combination of high distortion rate and low infiltration index suggest strong sol (molten slag) resistant ability.

Data taken by the mercury porosimeter are shown in Table 4 and pore diameter distribution curves of various samples are illustrated by Figs. 1 and 2. As can be seen in the two figures, the sol impregnated samples have narrower pore distribution, compared with prior to the impregnation; and Table 4 suggests, even with the treatment at 1550 °C to the impregnated samples, the infiltration index declines while the distortion rate climbs up, proving that the sol impregnation improves the material microstructure noticeably. At the same time, substantial decreases are found in the number of pores greater than 12 μm in the sol impregnated samples. In the case of the mixed sol impregnated samples which have been dried at 110 °C, the percentage of pores with diameters larger than 12 μm plunged to 18.64% from 89.52% prior to the impregnation; and in the case of the single sol impregnated sample, the percentage dropped to 21.69%. Accompanying the climbing temperature, pore diameters enlarge. Such being the case, for the mixed sol impregnated samples, the percentage of pores with diameters less than 12 μm plunged to 27.55% at 1550 °C from 81.36% at 110 °C; and for the single sol impregnated samples, the percentage dropped to 24.20% at 1550 °C from 78.31% at

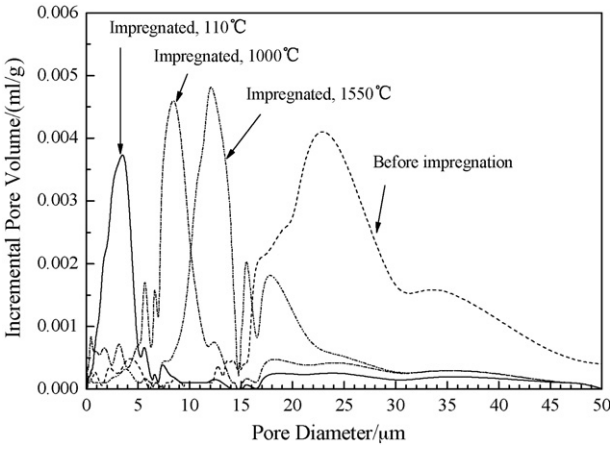

Fig. 1. Pore diameter distribution before and after impregnation by single sol.

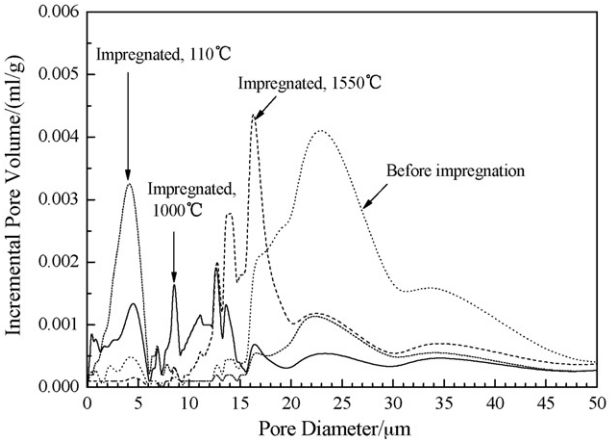

Fig. 2. Pore diameter distribution before and after impregnation by mixed sol.

110 °C. That the percentages of pores with diameter less than 12 μm at 1550 °C can be accounted for by the decomposition of $Cr(OH)_3$ under high temperature and the evaporation of Cr.

Fig. 3 shows SEM micrographs of the samples after and before the impregnation. Fig. 3a shows that pores of the un-impregnated samples have diameters within the range of 10–20 μm; Fig. 3b and c, displaying the microstructure of the samples impregnated in the single sol and in the mixed sol, respectively, show differences in the microstructures of the differently impregnated in samples. Fig. 3b distinctly depicts the pores interior filled with large quantities of lumpy-floss-like substances (principally $Cr(OH)_3$); in contrast, Fig. 3c demonstrates the filling substances mainly constituted by the mixture of $Cr(OH)_3$ and $Mg(OH)_2$. Fig. 3d illustrates $Cr(OH)_3$ in the pores, after the treatment at 1000 °C, decomposes into Cr_2O_3, which would grow in size. Lastly, filling substances described in Fig. 3e mainly comprise $MgCr_2O_4$. Therefore, after the treatment at 1000 °C, the filling substances in the pores are chiefly made up by Cr_2O_3 or $MgCr_2O_4$.

3.3. Slag resistance before and after impregnation

According to Section 2.3, prior to the experiment the test samples have to be heat-treated at 110 °C for 24 h, thereby ensuring the reaction described by Eqs. (2)–(4) be completely. After treated at 1600 °C, the samples were cut into halves.

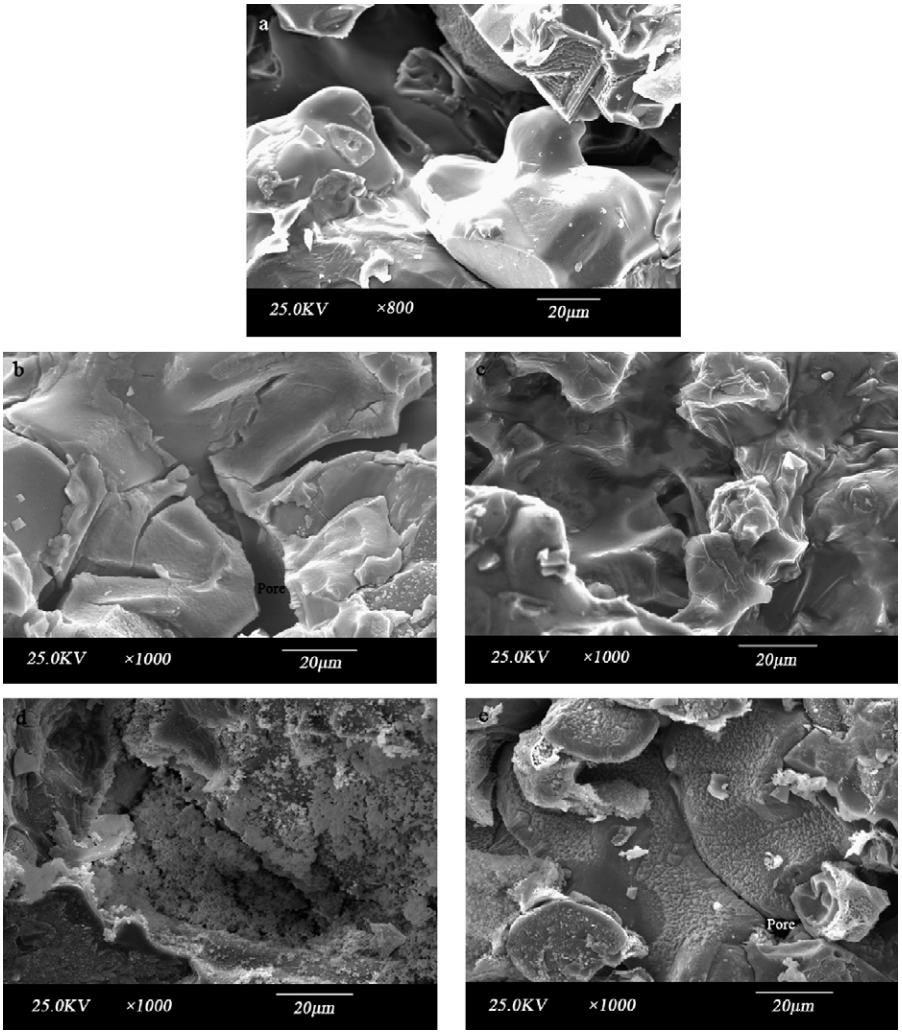

Fig. 3. SEM images of sections of specimens before and after impregnation: (a) untreated sample, (b) impregnated by single sol and dried at 110 °C, (c) impregnated by a mixed sol and dried at 110 °C, (d) impregnated by single sol and heat-treated at 1000 °C, (e) impregnated by mixed sol and heat-treated at 1000 °C.

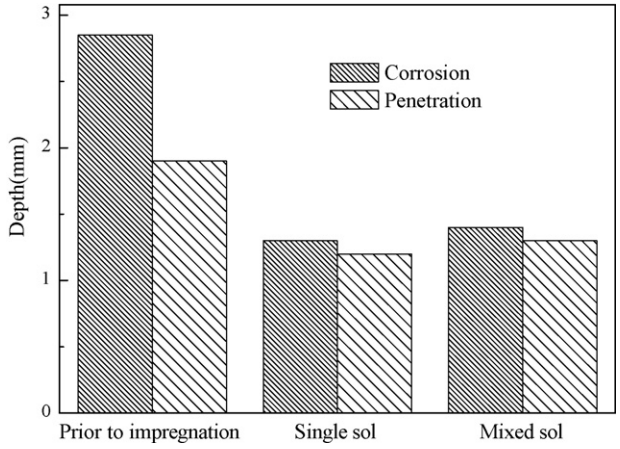

Fig. 4. Slag corrosion and penetration of magnesia-chrome bricks (before and after impregnation) tested at 1600 °C for 3 h in air.

Along the slag/refractory interface, the maximum corrosion depth and the maximum slag infiltration depth were measured, with the results from the same two samples averaged. Fig. 4 shows the mean corrosion depth and infiltration depth; Fig. 5 gives digital photos of the samples impregnated in the two sols and un-impregnated.

According to Fig. 4, the un-impregnated samples show a mean slag resistance change of 2.85 mm along the direction of radius while the single sol impregnated samples and the mixed sol impregnated samples show changes of 1.3 and 1.4 mm, respectively. Therefore, Figs. 4 and 5 bear evidence to the relatively poor slag resistance of un-impregnated samples and the improved slag resistance of the samples treated with the sol vacuum impregnation. In addition, in spite of the fact that the single sol impregnated samples fail to see the pore diameters improved the way as the mixed sol impregnated samples do, they still enjoy a corrosion resistance superior to those impregnated in the mixed sol.

Chen et al. [14] noted that there existed a reliable linear relation between the refractories corrosion resistance and the fractal dimension of the micro-boundary. And the fractal theory based concept, refractory fractal dimension R_f (refractory fractal), was advanced by them for evaluating the corrosion resistance of refractories. By measuring the corrosion boundary curve on the test samples, the fractal dimension was calculated. Since the parameter for the refractories service life does not consist in the mean corrosion thickness but the local maximum corrosion thickness (depth), the R_f value obtained from measuring the corrosion boundary curve can be used to evaluate the slag resistance of the refractories. With the aid of the box-counting method [15], $N(\varepsilon)$ grids with the side length ε are used to cover the contour curve. Between $N(\varepsilon)$ and the fractal dimension D there exists a relation as described in Eq. (5):

$$N(\varepsilon) = C\varepsilon^{-D} \tag{5}$$

where C is a proportionality constant and D is refractory fractal.

Using grids with the side length ε to cover the entire fractal image, the total number $N(\varepsilon)$ of the grids occupied by the image

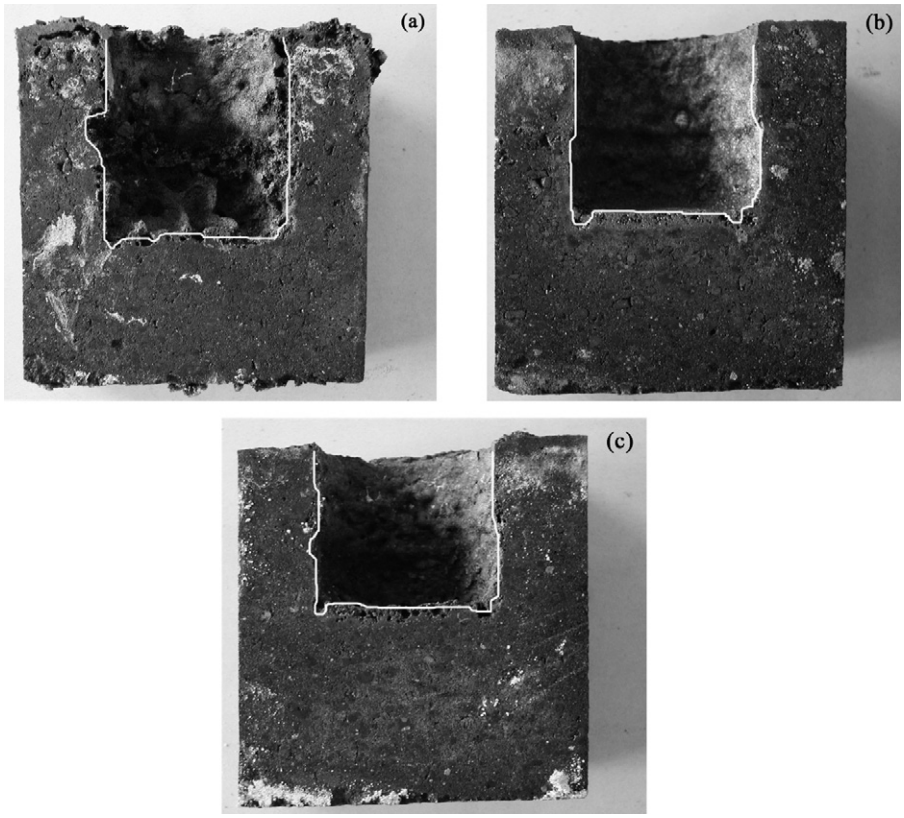

Fig. 5. Photographs of section of corroded samples: (a) untreated sample; (b) impregnated by single sol; (c) impregnated by mixed sol after exposure to copper converter slag.

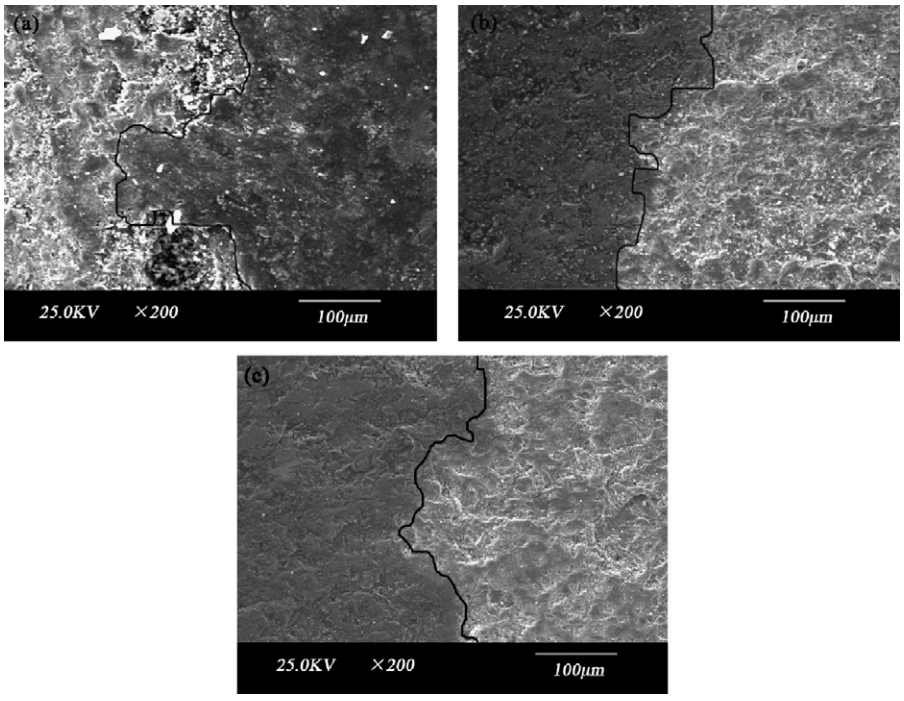

Fig. 6. SEM images and corresponding micro-boundary curves of polished section of corroded samples before and after impregnation: (a) untreated sample; (b) impregnated by single sol; (c) impregnated by mixed sol.

is worked out. As lg $N(\varepsilon)$ is drawn with lg ε, the line's slope equals the fractal dimension, i.e. D value.

Shown in Fig. 6 are SEM micrographs of the samples before and after impregnation and the corresponding micro corrosion boundary curves. On the basis of Fig. 6 and Eq. (5), $D = 1.0937$ is obtained from the un-impregnated samples, while the corresponding D values of the single sol impregnated and mixed sol impregnated are 1.0744 and 1.0761, respectively. The closer the D value to 1, the better the corrosion resistance [14]. Based on the results afforded by these calculations, we come to the conclusion that sol impregnation can improve the corrosion resistance of the magnesia-chrome bricks and the single sol impregnation delivers a better effect.

According to Eq. (1), the infiltration depth is inversely proportional to the molten mass viscosity and contact angle, and in direct proportion to the surface tension. Under the same conditions of molten slag corrosion, the interior surface of the pores of the sol impregnated samples is filled with penetrating Cr_2O_3 and $MgCr_2O_4$ and content of MgO and Cr_2O_3 around the pores increases simultaneously. At the time the molten slag passes through pores, Cr_2O_3 and $MgCr_2O_4$ are the first to react with the slag and absorb S and Cu contained in the slag, thereby increasing the molten slag viscosity and slowing down slag further penetration. As a consequence, the sol impregnation has improved the corrosion resistance of the magnesia-chrome bricks. On the other hand, as a higher content of Cr_2O_3 will lead to a larger contact angle θ [9], high content of Cr_2O_3 in the pore passage of the single sol impregnated samples results in a decreased surface tension of $FeO–SiO_2$ used for tying slag, which accounts for the diminished slag infiltration ability. This explains why the single sol impregnated samples provide a better corrosion resistance.

4. Conclusions

Two kinds of nanosized chrome-bearing sols fabricated by homogeneous precipitation, i.e. Cr_2O_3 precursor sol and $MgCr_2O_4$ spinel precursor sol, were vacuum impregnated in magnesia-chrome bricks. As the nanosized particles in the two sols infiltrated into the magnesia-chrome bricks pores, they improved the Cr_2O_3 content and the bulk density and decreased the apparent porosity as compared to un-impregnated sample. For untreated samples, the percentage of pores with diameters greater than 12 μm was 89.52%; for the samples impregnated by the single sol, the percentages of pores with diameter greater than 12 μm dropped to 21.69% and 75.80%, after heat-treatment at 110 and 1550 °C, respectively; and for the samples impregnated by mixed sol, the percentages declined to 18.64% and 72.45%, respectively. After heat-treatment at 1550 °C, the pore number increased because the infiltrating substances, $Cr(OH)_3$ or $Mg(OH)_2$, decomposed or Cr evaporated at high temperature. Next, the un-impregnated samples and the samples impregnated by the two sols were put under the same conditions for the static crucible test, analyzing the slag corrosion depth and infiltration depth. Results show that both sols could improve the magnesia-chrome bricks corrosion resistance in impregnation, with the single sol producing a better result. The improved corrosion resistance was ascribable to the fact that penetrating hydroxides formed Cr_2O_3 or $MgCr_2O_4$ at high temperature, which adhered to the pores internal wall and decreased the pores diameter, thereby minifying the slag corrosion passage; additionally, the increased content of Cr_2O_3 further decreased the wetting angle of the materials and the molten slag, eventually enhancing the corrosion resistance performance. As the actual operating

temperature of the copper smelting furnace ranges between 1200 and 1300 °C, we may expect that applying copper smelting furnace magnesia-chrome bricks to vacuum impregnation can improve their corrosion resistance.

References

[1] M.K. Haldar, H.S. Tripathi, S.K. Das, A. Ghosh, Effect of compositional variation on the synthesis of magnesite–chrome composite refractory, Ceram. Int. 30 (2004) 911–915.
[2] Y. Li, The Application Study of Performance Magnesia-chrome Refractory, University of Science and Technology Beijing, 2002, pp. 87–89.
[3] J.L. Liow, P. Tsirikis, N.B. Gray, Study of refractory wear in the tuyere region of a Peirce-Smith nickel convertor, Can. Metall. Quart. 2 (37) (1998) 99–117.
[4] L. Bradley, L. Li, F.H. Stott, Surface modification of alumina-based refractories using a xenon arc lamp, Appl. Surf. Sci. 154/155 (2000) 675–681.
[5] M. Rosso, A. Scrivani, D. Ugues, et al., Corrosion resistance and properties of pump pistons coated with hard materials, Int. J. Refract. Met. Hard Mater. 19 (2000) 45–52.
[6] Z.-Z. Zhu, J.-Q. He, Modern Copper Metallurgy, vol. 1, Science Press, Beijing, 2003, pp. 485–487.
[7] S.M. D'Alfonzo, Vacuum impregnation [J], Met. Finish. 1 (98) (2000) 510–512.
[8] Z.-Q. Guo, Laboratory slag tests of refractory corrosion [J], Naihuo Cailiao 23 (2) (1989) 55–60.
[9] H.-Z. Wang, Y.-Y. Deng, H.-Z. Zhao, et al., A method of being improved properties of magnesia-based refractories and the corresponding products by using this method [P]. CN200510018955.0.
[10] Y.-B. Wang, Manufacture of vacuum impregnation apparatus for magnesite-chrome refractory brick [J], Naihuo Cailiao 34 (4) (2000) 274.
[11] Y.-Y. Deng, H.-Z. Wang, P.-H. Li, et al., Synthesis of nanosized magnesium-chrome spinel powders by coprecipitation method [J], Wujiyan Gongye 37 (7) (2005) 32–35.
[12] S.-L. Yang, Magnesia of high hydration resistance [J], Foreign Refract. 22 (6) (1997) 14–18.
[13] A. Carlos, L.Y. Léon, New perspectives in mercury porosimetry [J], Adv. Colloid Interf. Sci. 76/77 (1998) 341–372.
[14] S.-H. Chen, Y.-R. Hong, J.-L. Sun, Research on refractories corrosion fractal based on the fractal characteristics of micro boundary [J], Naihuo Cailiao 37 (2) (2003) 78–81.
[15] B.B. Mandelbrot, The Fractal Geometry of Nature [M], 2nd ed., W.H. Freeman Co., San Francisco, 1983.